Journal of Applied Mathematics and Physics, 2020, 8, 1374-1401
https://www.scirp.org/journal/jamp
ISSN Online: 2327-4379
ISSN Print: 2327-4352

The Lie Group $SU(2)$ Hopf Fibration and the Fourier Equation

Adelin Mulenda Mbuto[1], Lucien Zihindula Biguru[2], Jean Masudi Kalongama[3], Joseph Cimbela Kabongo[1], Albert Kabasele Yenga-Yenga[1]

[1]National Pedagogical University/Kinshasa, Kinshasa/Binza, Democratic Republic of the Congo
[2]Official University of Bukavu/Bukavu, Sud-Kivu/Bukavu, Democratic Republic of the Congo
[3]Institut Supérieur Pédagogique/Bukavu, Sud-Kivu/Bukavu, Democratic Republic of the Congo
Email: adelinmulenda@gmail.com

How to cite this paper: Mulenda Mbuto, A., Zihindula Biguru, L., Masudi Kalongama, J., Cimbela Kabongo, J. and Kabasele Yenga-Yenga, A. (2020) The Lie Group $SU(2)$ Hopf Fibration and the Fourier Equation. *Journal of Applied Mathematics and Physics*, **8**, 1374-1401.
https://doi.org/10.4236/jamp.2020.87105

Received: May 19, 2020
Accepted: July 24, 2020
Published: July 27, 2020

Abstract

The Fourier equation explains the dynamics of heat transfer. But bringing this phenomenon closer to the notion of fibration seems difficult to achieve. This study then aims to find the solution of the one-dimensional Fourier equation and to interpret it in terms of bundle. And then apply the results obtained at the Kankule site in Katana in South Kivu. To do this work, we resorted to geometric or topological analysis of the Hopf fibration of the unit sphere S^3 (identifiable in $SU(2)$). We had taken the temperatures of the thermal waters and the soil of Kankule, from 2010 to 2014, *in situ*. And laboratory analyses had allowed us to know the physical and chemical properties of the soil and water at each of our 14 study sites in Kankule. The data of the geomagnetic field of each site, were taken in on the site NOAA, for our period of study. We then determined the integral curve (geotherm) of the Fourier equation and wrote it as a unit quaternion which is a bundle. The constants intervened in the geotherm, for each site of Kankule, we had obtained them statistically. We have found that the geotherm of each Kankule site is a bundle. We have compared this model to the bundle model of the geomagnetic field. From there we realized that to determine the energy potential of Kankule, we should consider the thermal springs separately. We were able to find a connection between the fibration of the geomagnetic field and the heat field for the Kankule site.

Keywords

Fiber, Hopf Fiber, Geotherm, Quaternion, Geomagnetic Field and Potential Energy

1. Conceptual Fame

1.1. The Quaternions and the Sphere Unit S^3

1.1.1. Quaternions

1) Definitions

In $\mathbb{R}^4$, consider $q=(a,b,c,d)=(a,\boldsymbol{u})$ and $q'=(a',b',c',d')=(a',\boldsymbol{v})$; for $\boldsymbol{u}=(b,c,d)$ and $\boldsymbol{v}=(b',c',d')$ in $\mathbb{R}^3$. The addition and multiplication in $\mathbb{R}^4$ are defined by the relations below [1] [2] [3]:

$$q+q'=(a+a',\boldsymbol{u}+\boldsymbol{v}) \tag{1}$$

with $\boldsymbol{u}+\boldsymbol{v}$ the vector addition in $\mathbb{R}^3$, and

$$\begin{aligned} q*q' &= (aa'-bb'-cc'-dd', ab'+bb'+cd'-dc', \\ &\quad ac'+ca'-bd'+db', ad'+da'+bc'-cb') \\ &= (aa'-\boldsymbol{u}\cdot\boldsymbol{v}, a\cdot\boldsymbol{v}+a'\cdot\boldsymbol{v}+\boldsymbol{u}\wedge\boldsymbol{v}) \end{aligned} \tag{2}$$

where $\boldsymbol{u}\cdot\boldsymbol{v}$ and $\boldsymbol{u}\wedge\boldsymbol{v}$ are respectively the scalar product and the vector product in $\mathbb{R}^3$. We verify that $(\mathbb{R}^4,+,*)$ is a commutative body, called the quaternion body. We mark it *H*, in honor of Hamilton who built it first.

We have $\overline{q}=(a,-\boldsymbol{u})$ as a conjugate of *q*, and $-q=(-a,-\boldsymbol{u})$ being the opposite of *q*. The norm of *q* is

$$|q|=\sqrt{q*\overline{q}}=\sqrt{a^2+b^2+c^2+d^2} \tag{3}$$

The inverse of *q* is

$$q^{-1}=\frac{\overline{q}}{|q|} \tag{4}$$

We denote [4] [5] [6]

$$1=(1,0,0,0), i=(0,1,0,0), j=(0,0,1,0) \text{ and } k=(0,0,0,1). \tag{5}$$

and

$$i^2=j^2=k^2=-1=i*j*k \tag{6}$$

with $ij=k=-ji$; $jk=i=-kj$ and $ki=j=-ik$. *H* is a vector space on *R* whose basis is $(1,i,j,k)$. Thus the quaternion

$$q=(a,b,c,d)=a+b*i+c*j+d*k \tag{7}$$

The set of pure quaternions is

$$\mathbb{H}_{pur}=\{p\in H / p=(0;b;c;d);(b;c;d)\in\mathbb{R}^3\} \tag{8}$$

We identify $\mathbb{H}_{pur}$ with $\mathbb{R}^3$. We check that if $p\in\mathbb{H}_{pur}$, then $p=-\overline{p}$. So for $p\in H$ which is such that $p^2=-1$, we will have $|p|=1$ and $p=-\overline{p}$, which implies that $p\in\mathbb{H}_{pur}$.

2) Theorem 1

Any quaternion *q* can be written as

$$q=|q|(\cos\theta+p\sin\theta) \tag{9}$$

with $\theta \in R$ and $p \in \mathbb{H}_{pur}$ [1] [3].

Indeed, $q/|q| = (a;b;c;d)$ is a quaternion of module 1, then $a \in [-1;1] \cap R$ because $|q/|\overline{q}|| = \sqrt{a^2+b^2+c^2+d^2} = 1$. There then exists $\theta \in R$ such that $a = \cos\theta$ and $\sqrt{b^2+c^2+d^2} = \sin\theta$. When θ is not a multiple of π, we set $p = \dfrac{\dfrac{q}{|q|} - \cos\theta}{\sin\theta}$, a pure quaternion of norm 1 and whose square is −1. When θ is a multiple of π, we immediately have the result stated by the theorem, whatever the pure quaternion considered.

1.1.2. The S^2 and S^3 Spheres

A) Definitions

The unit sphere S^n, of dimension n, of $\mathbb{R}^{n+1}$ is defined by [2] [7] [8]:

$$S^n = \left\{(x_0;x_1;\cdots;x_n) \in \mathbb{R}^{n+1} / \sum_{i=0}^{0} x_i^2 = 1\right\} \tag{10}$$

Thus S^3 is the part of $\mathbb{R}^4$ defined by

$$S^3 = \left\{(a,b,c,d) \in \mathbb{R}^4 / a^2+b^2+c^2+d^2 = 1\right\} \tag{11}$$

and S^2 the part of $\mathbb{R}^3$ defined by

$$S^2 = \left\{(x,y,z) \in \mathbb{R}^3 / x^2+y^2+z^2 = 1\right\} \tag{12}$$

Note $S'(0,0,-1)$ and $N'(0,0,1)$ are respectively the south and north poles of S^2. Consider the open sets $U_{N'} = S^2 \setminus \{N'\}$ and $U_{S'} = S^2 \setminus \{S'\}$. Let the applications, called stereographic projections, be as follows:

$$\psi_{N'} : U_{N'} \to \mathbb{R}^2, \text{ with } \psi_{N'}(x,y,z) = \left(\frac{x}{1-z}, \frac{y}{1-z}\right); \tag{13}$$

and

$$\psi_{S'} : U_{S'} \to \mathbb{R}^2, \text{ with } \psi_{S'}(x,y,z) = \left(\frac{x}{1+z}, \frac{y}{1+z}\right). \tag{14}$$

We find $\{(U_{N'},\psi_{N'});(U_{S'},\psi_{S'})\}$ a differentiable atlas of S^2.

This method, of stereographic projection, makes it possible to obtain a differentiable structure for any sphere S^n.

For $n = 3$, the stereographic projections give for S^3 the atlas $\{(U_N,\varphi_N);(U_S,\varphi_S)\}$; where $U_N = S^3 \setminus \{(0,0,0;1)\}$ and $U_S = S^3 \setminus \{(0,0,0;-1)\}$. We have

$$\varphi_N(a,b,c,d) = \left(\frac{b}{1-a}, \frac{c}{1-a}, \frac{d}{1-a}\right) \tag{15}$$

and

$$\varphi_S(a,b,c,d) = \left(\frac{b}{1+a}, \frac{c}{1+a}, \frac{d}{1+a}\right) \tag{16}$$

B) Link between H and $SU(2)$

1) Definitions

$$
\begin{aligned}
SU(2) &= \{M \in U(2) / \det M = 1\} \\
&= \left\{ M = \begin{pmatrix} a+ib & c+id \\ -c+id & a-ib \end{pmatrix} / a^2+b^2+c^2+d^2 = 1; (a,b,c,d) \in \mathbb{R}^4 \right\} \\
&= \left\{ M = \begin{pmatrix} Z_1 & Z_2 \\ -Z_2 & Z_1 \end{pmatrix} / |Z_1| + |Z_2| = 1; (Z_1, Z_2) \in \mathbb{C}^2, \right. \\
&\quad \left. Z_1 = a+ib; Z_2 = c+id; (a,b,c,d) \in \mathbb{R}^4 \right\} \\
&= \left\{ M \in GL(2,\mathbb{C}) M\bar{M}^t = 1 = \bar{M}^t Met |M| = 1 \right\}
\end{aligned} \tag{17}
$$

[2] [4] [5].

SU(2) is then identified with group S^3, quaternions of module 1. Indeed; consider the homeomorphism f defined as below:

$$f : SU(2) \to S^3;$$

with

$$\begin{pmatrix} Z_1 & Z_2 \\ -Z_2 & Z_1 \end{pmatrix} \to f\left(\begin{pmatrix} Z_1 & Z_2 \\ -Z_2 & Z_1 \end{pmatrix} \right) = \begin{pmatrix} 1 & 0 \end{pmatrix} \begin{pmatrix} Z_1 & Z_2 \\ -Z_2 & Z_1 \end{pmatrix} = \begin{pmatrix} Z_1 & Z_2 \end{pmatrix}.$$

Thanks to *f* we identify *SU*(2) with S^3. We then consider *SU*(2) as a sub-body S^3 of *H*, quaternions of module 1

2) Links between *SU*(2) * *U*(1) and *U*(2) as well as between *SO*(3) and *SU*(2)

a) Theorem2 "Links between *SU*(2) * *U*(1) and *U*(2)"

$$U(2) \approx \frac{SU(2) * U(1)}{Z_2} \tag{18}$$

With $I_{2\times 2} = \begin{pmatrix} 1 & 0 \\ 0 & 1 \end{pmatrix}$, $-I_{2\times 2} = \begin{pmatrix} -1 & 0 \\ 0 & -1 \end{pmatrix}$ and $Z_2 = \{(I_{2\times 2}, 1); (-I_{2\times 2}, -1)\}$ [2], [4] and [5].

***Proof of Theorem* 2**

We find that $\forall M \in SU(2)$ and $\forall q \in Z_2$: $q * M = M * q$. We have Z_2 a distinguished (or normal) subgroup of *SU*(2) because $\forall q \in Z_2$;

$q * SU(2) * q^{-1} = SU(2)$

i) Let

$$f : SU(2) * U(1) \to U(2); \ (M, e^{i\theta}) \to f(M, e^{i\theta}) = e^{i\theta} * M$$

We check that *f* is a surjective homomorphism, whose kernel is

$Kerf = Z_2 = \{(I_{2\times 2}, 1); (-I_{2\times 2}, -1)\}$ and *Imf* = *U*(2).

Consequently *Imf* is isomorphic to (*SU*(2) * *U*(1))/*Kerf*. *I.e.* *U*(2) ≈ (*SU*(2) * *U*(1))/(*Kerf*)

b) Theorem 3 "Links between *SO*(3) and *SU*(2)"

The group *SO*(3) is isomorphic to the quotient of *SU*(2) by its center. The center of *SU*(2) is $Z_2 = \{I_{2\times 2}, -I_{2\times 2}\}$, with $I_{2\times 2} = \begin{pmatrix} 1 & 0 \\ 0 & 1 \end{pmatrix}$ and $-I_{2\times 2} = \begin{pmatrix} -1 & 0 \\ 0 & -1 \end{pmatrix}$ [2] [4].

Let us demonstrate $SO(3) \approx (SU(2))/(Z_2)$ in the following three steps:

1st step: We will establish a homomorphism $g: SU(2) \to SO(3)$

2nd step: We will prove that g is surjective

3rd step: We will then show from $Kerg = Z_2$

Proof of Theorem 3

ii)

$$\begin{aligned} &R_{-q}: \left(\mathbb{H}^*, .\right) \to \left(\mathbb{H}^*, .\right) \text{ with } \mathbb{H}^* = \left\{q \in \mathbb{H} / q \neq 0\right\}; \\ &\text{and } p \to R_q(p) = q * p * \overline{q} \end{aligned} \tag{19}$$

We find that R_q is a bijection. It is called conjugation by the element q of the multiplicative group $\mathbb{H}^*$. We find that $\left(\mathbb{H}_{pur}, .\right)$ is a subgroup of $\left(\mathbb{H}^*, .\right)$.

We make the identification of $\mathbb{H}_{pur}$ ur and $\mathbb{R}^3$, thanks to the following bijection ζ:

$$\zeta: \mathbb{H}_{pur} \to \mathbb{R}^3; (0; x; y; z) \to \zeta\left((0; x; y; z)\right) = (x; y; z) \tag{20}$$

Thus $\forall q = M \in SU(2)$, we verify that $R_q: \mathbb{H}_{pur} \to \mathbb{R}^3$ given by

$$m \to R_q(m) = q * m * q^{-1} = q * m * \overline{q} \tag{21}$$

Let us show that this restriction of R_q, to $\mathbb{H}_{pur}$ or $\mathbb{R}^3$, is a rotation. Indeed:

1˚) $\forall m_1, m_2 \in \mathbb{H}_{pur}$; and $\forall \alpha, \beta \in R$:

$R_q(\alpha * m_1 + \beta * m_2) = \alpha * R_q(m_1) + \beta * R_q(m_2)$

2˚) $\forall q \in SU(2)$; $\forall m \in \mathbb{H}_{pur}$, we find $\overline{m} = -m$ *i.e.* $\overline{m} + m = 0$

So $R_q(m) + R_q(\overline{m}) = 0$ because

$$\begin{aligned} R_q(m) + R_q(\overline{m}) &= q * m * \overline{q} + \overline{q * m * \overline{q}} = q * m * \overline{q} + \overline{\overline{q}} * \overline{m} * \overline{q} \\ &= q * m * \overline{q} + q * \overline{m} * \overline{q} = q * (\overline{m} + m) * \overline{q} = q * 0 * \overline{q} = 0 \end{aligned}$$

The matrix of R_q is therefore a regular matrix

3˚) Let on H be the standard map $\mathfrak{n}$

$$n: \mathbb{H} \to \mathbb{R}^+; p \to \mathfrak{n}(p) = \sqrt{p * \overline{p}} \tag{22}$$

We verify that

$$\begin{aligned} n\left(R_q(p)\right) &= \mathfrak{n}(q * p * \overline{q}) = \mathfrak{n}(q) * \mathfrak{n}(p) * \mathfrak{n}(\overline{q}) = \mathfrak{n}(p) * \mathfrak{n}(q) * \mathfrak{n}(\overline{q}) \\ &= \mathfrak{n}(p) * \mathfrak{n}(q * \overline{q}) = \mathfrak{n}(p) * \mathfrak{n}(1) = \mathfrak{n}(p) * 1 = \mathfrak{n}(p) \end{aligned}$$

Consequently $\forall q \in SU(2)$, we find that R_q is an orthogonal isomorphism of H; and therefore its restriction to $\mathbb{H}_{pur}$, (or $\mathbb{R}^3$) is an isometry. In other words: $\forall q \in SU(2)$, we find $R_q \in O(3)$.

4˚) As $\forall q \in SU(2)$, $\det R_q = 1$; then R_q is a rotation of $\mathbb{R}^3$; *i.e.* $R_q \in N / SO$ (3).

Thus $g: SU(2) \to SO(3)$; $q \to g(q) = R_q$; is an application which associates each element q with its rotation matrix R_q.

Like $\forall q_1, q_2 \in SU(2)$, we have R_{q_1} o $R_{q_2} = R_{q_1 * q_2}$ and

$$g(q_1 * q_2) = R_{q_1} \text{ o } R_{q_2} = R_{q_1} * R_{q_2}; \tag{23}$$

then g is a group morphism.

We find that $Kerg = Z_2 = \{I_{2\times 2}, -I_{2\times 2}\}$.

And as $Img = g(SU(2)) = SO(3)$; because $\forall R_q \in SO(3)$, $\exists q \in SU(2)$ such that $g(q) = R_q$ (that is to say g is surjective); then $Img = (SU(2))/(Kerg)$. In other words $SO(3) \approx (SU(2))/(\{I_{2\times 2}, -I_{2\times 2}\})$.

c) Theorem 4 "Links between $U(1)$ and $SU(2)$"

$U(1)$ is a multiplicative subgroup of $SU(2)$ [4] and [5].

Proof of Theorem 4

We have $U(1) = \{z \in C / z = e^{i\theta}, \theta \in R\}$. $U(1)$ is a group of complex numbers of modules 1. We find the following isomorphisms f_1 and f_2:

$$f_1 : U(1) \to SO(2); \text{ with } e^{i\theta}, \to \begin{pmatrix} \cos\theta & -\sin\theta \\ \sin\theta & \cos\theta \end{pmatrix} \tag{24}$$

and;

$$f_2 : U(1) \to S^1; \text{ with } e^{i\theta}, \to (\cos\theta, \sin\theta) \tag{25}$$

These isomorphisms identify $U(1)$ with $SO(2)$, or the unit sphere S^1 of $\mathbb{R}^2$.

The immersion of S^1 in S^3 allows to consider $U(1)$ as a subgroup of $SU(2)$.

1.2. Rotation Dies and Sphere S_3

1.2.1. Geometric Interpretation of a Quaternion

1) Theorem 5

Let q be any non-zero quaternion; noted

$$q = |q|(\cos\theta + p\sin\theta) \tag{26}$$

with $\theta \in R$ and $p \in \mathbb{H}_{pur}$. Then the application R_q u is a rotation of angle 2θ and of vector p [1] [3] [5] [6].

Proof of Theorem 5

By demonstrating Theorem 3, we have seen that $\forall q = M \in SU(2)$, we check that R_q: $\mathbb{H}_{pur} \to \mathbb{R}^3$ given by $m \to R_q(m) = q * m * q^{-1} = q * m * \overline{q}$; R_q is a rotation, thanks to relations (21) and (22).

Let us use relations (2), (9), (21) and (22) to determine the angle of rotation R_q and his axis.

According to (9), we have $q = |q|(\cos\theta + p\sin\theta) = \cos\theta + p\sin\theta$, because $\forall q \in S^3$, $|q| = 1$ and that $p \in \mathbb{H}_{pur}$, then $p^2 = p * p = -1$, Thus

$$\begin{aligned} R_q(m) &= q * m * q^{-1} = q * m * \overline{q} = (\cos\theta + p\sin\theta) * m * (\cos\theta - p\sin\theta) \\ &= (\cos^2\theta) * m + 2(\sin\theta\cos\theta) * (p \text{ л } m) - (\sin^2\theta) * [m - 2 * p * (m \cdot p)] \end{aligned} \tag{27}$$

Since $\begin{cases} m * p = (-m \cdot p, m \text{ л } p) = -m \cdot p + m \text{ л } p \\ p * m - m * p = 2p \text{ л } m \end{cases}$, then

$$\begin{aligned} R_q(m) &= (\cos^2\theta) * m + (\sin 2\theta) * (p \text{ л } m) + (2\sin^2\theta) * [(p \cdot m) * p] - (\sin^2\theta) * m \\ &= (\cos 2\theta) * m + (\sin 2\theta) * (p \text{ л } m) + (2\sin^2\theta) * [(p \cdot m) * p] \end{aligned} \tag{28}$$

Which allows to deduce:

a) If $m = p$, then $R_q(m) = R_q(p) = p$ since

$$\begin{cases} p \perp m = 0 \\ p \cdot m = m \cdot p = 1 \end{cases} \tag{29}$$

As p is invariant by R_q, then p is a vector of the axis of rotation of R_q

b) If p is perpendicular to m, then $p \cdot m = 0$. It then comes that

$$R_q(m) = (\cos 2\theta) * m + (\sin 2\theta) * (p \perp m) \tag{30}$$

By comparing this relation to (9), we conclude that R_q is a rotation of angle 2θ, and of axis p.

Theorem 5 is therefore proven.

We therefore observe that a quaternion q is also a rotation of angle θ, and of axis p.

2) Matrix of a rotation R_q of an element q of $SU(2)$ or S^3

Consider the following matrices in SU (2) [5] [6] [9] [10] [11]:

$\sigma_0 = \begin{pmatrix} 1 & 0 \\ 0 & 1 \end{pmatrix}$; $\sigma_1 = \begin{pmatrix} 0 & 1 \\ 1 & 0 \end{pmatrix}$; $\sigma_2 = \begin{pmatrix} 0 & -i \\ i & 0 \end{pmatrix}$; and $\sigma_3 = \begin{pmatrix} 1 & 0 \\ 0 & -1 \end{pmatrix}$, the last 3 of which are Pauli matrices. Note $\boldsymbol{\sigma} = i\sigma_1 + j\sigma_2 + k\sigma_3 = (\sigma_1; \sigma_2; \sigma_3)$. Since $\boldsymbol{u}$ is a unitary matrix of $SU(2)$, and properties of the Pauli matrices, we find $(\boldsymbol{u}\cdot\boldsymbol{\sigma})^2 = \sigma_0 = (\boldsymbol{u}\cdot\boldsymbol{\sigma})^{2n}$ and $(\boldsymbol{u}\cdot\boldsymbol{\sigma})^{2n+1} = \boldsymbol{u}\cdot\boldsymbol{\sigma}$; $\forall n \in N$. Consequently

$$\begin{aligned} q &= \exp\{-i\theta \boldsymbol{u}\cdot\boldsymbol{\sigma}\} \\ &= \sigma_0 - i(\theta)(\boldsymbol{u}\cdot\boldsymbol{\sigma}) - (\theta)^2 \frac{(\boldsymbol{u}\cdot\boldsymbol{\sigma})^2}{2!} + i(\theta)^3 \frac{(\boldsymbol{u}\cdot\boldsymbol{\sigma})^3}{3!} \\ &\quad + \cdots + i(\theta)^n \frac{(\boldsymbol{u}\cdot\boldsymbol{\sigma})^n}{n!} + \cdots \\ &= \sigma_0 \cos\theta - i(\boldsymbol{u}\cdot\boldsymbol{\sigma})\sin\theta = U(\boldsymbol{u},\theta) \end{aligned}$$

We then find that a rotation q of angle θ in $S^3 = SU(2)$ corresponds to a rotation of angle 2θ in S^2. The matrix form of this rotation q is given by the relation:

$$q = U(\boldsymbol{u},\theta) = \begin{pmatrix} \cos\theta - iu_z \sin\theta & -(iu_x + u_y)\sin\theta \\ (-iu_x + u_y)\sin\theta & \cos\theta + iu_z \sin\theta \end{pmatrix} \tag{31}$$

With $\boldsymbol{u}$ unit vector of $\mathbb{R}^4$ along the axis p of the relation (29). We also have in $\mathbb{R}^3$ the following unit vectors $\boldsymbol{u}_x = (1;0;0)$, $\boldsymbol{u}_y = (0;1;0)$, $\boldsymbol{u}_z = (0;0;1)$; with i imaginary unity. The relation (31) indicates to us that a quaternion is a rotation, in the space of 1/2-spinner. It is a rotation in space of rank 1 spinners.

1.2.2. Euler Angles of a Quaternion

Any matrix q of $SU(2)$ or S^3 can be decomposed, using Euler angles, as below [2] [4] [6]:

$$\begin{aligned} q &= \begin{pmatrix} e^{i\psi} & 0 \\ 0 & e^{-i\psi} \end{pmatrix} * \begin{pmatrix} \cos\theta & i\sin\theta \\ i\sin\theta & \cos\theta \end{pmatrix} * \begin{pmatrix} e^{i\varphi} & 0 \\ 0 & e^{-i\varphi} \end{pmatrix} \\ &= \begin{pmatrix} \cos\theta e^{i(\psi+\varphi)} & i\sin\theta e^{i(\psi-\varphi)} \\ i\sin\theta e^{-i(\psi-\varphi)} & \cos\theta e^{-i(\psi+\varphi)} \end{pmatrix} \end{aligned} \tag{32}$$

with $0 \le \theta \le \pi/2$; $0 \le \varphi \le \pi$ and $-\pi \le \psi \le \pi$.

The approach formulated by relations (31) and (32) is used in Quantum Mechanics, in the theory of angular momentum.

1.3. Fibration

1.3.1. Prelude

The total space $P = SU(2)$ from the topological point of view is identifiable with S^3. Consider a group $U(1)$, and perform a class decomposition of $SU(2)$ with respect to $U(1)$. For Let $g \in SU(2) \setminus U(1)$. We consider the set $\bar{g} = g * U(1) = \{g * w / w \in U(1)\}$. Then we consider an element k of $SU(2)$, which is neither in $U(1)$, nor in $\bar{g}$. We build the set $\bar{k} = k * U(1) = \{k * h / h \in U(1)\}$. We continue the process of class construction in $SU(2) \setminus U(1)$. In order to account, we succeed in writing $SU(2)$ as an infinite union of classes of the type $\bar{g} = g * U(1)$. The quotient set $SU(2)/U(1)$ obtained is identified at S^2. The group $P = SU(2) = S^3$ is considered to be an infinite union of circles $U(1) = S^1$; parameterized by the sphere $U(2) = S^2 = SU(2)/U(1)$ [Courses and Seminars (1)] (Figure 1).

The structural group $U(1)$ acts by multiplication on the right, on the total space $SU(2)$. We have chosen $U(1)$ as a distinguished subgroup of $SU(2)$. This fibration in circles of $S^3 = SU(2)$ is called Hopf fibration of $S^3 = SU(2)$ (Figure 2).

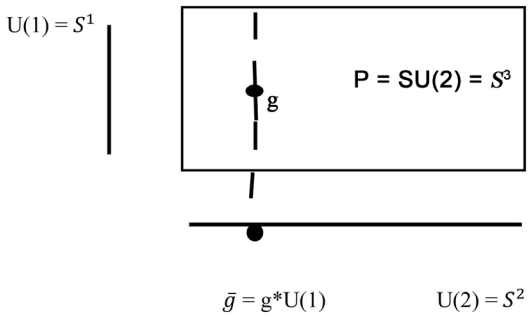

Figure 1. Fibration of $SU(2)$ in circles.

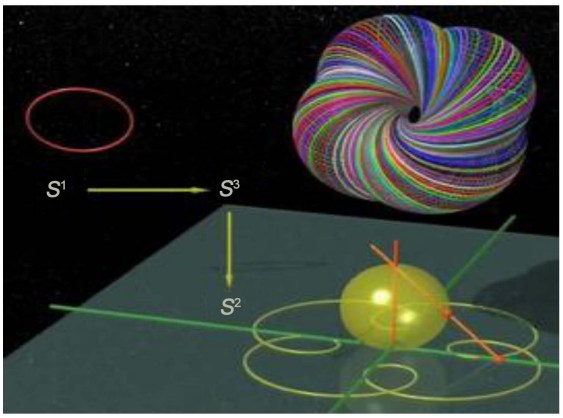

Figure 2. Hopf's fibration [12].

1.3.2. Hopf Fiber of a Lie G Group

1) Algebraic formulation

Let G be a Lie group, and H a Lie subgroup of G. We assume that H is closed in G, so that the topology of the quotient group G/H is separated. We consider the equivalence relation R defining the classes to the left of H. Thus two elements g and k of G are in relation R, if and only if $k \in \bar{g} = g * H$. Consider the application h, defined as below [2] [13]:

$$h: G \to G/H; g \to h(g) = \bar{g} = g * H. \tag{33}$$

The application h defines a main fibration. Any group G is thus a principal fibered space above G/H. The structural group being H. The quotient set G/H, which is the basis of the bundle, is only a group if H is distinguished in G.

We use the notation $H \to G \to G/H$, to characterize a fibration h of G above G/H. In the previous paragraph, we then introduced this fibration $U(1) \to SU(2) \to SU(2)/U(1)$ (Figure 3).

2) Geometric and topological formulation

a) Definitions of this formulation

$$\text{Consider}(P; M; \pi) \text{ where } \begin{cases} P: \text{is a differential variety} \\ M: \text{is a differential variety} \\ \pi \square \text{he projection of } P \text{ onto } M \end{cases} \tag{34}$$

We say that P is a vector bundled space of base M, of projection π and of fiber-type $\mathbb{R}^n$ if:

i) $\forall m \in M$; $\pi^{-1}(m)$ is a vector space

ii) $\forall m \in M$; $\exists$ a neighborhood U of m and a diffeomorphism (35)

$$\psi: U * \mathbb{R}^n \to \pi^{-1}(U) \quad \text{such that} \quad \begin{cases} \text{(a) } \pi \circ \psi(m; \boldsymbol{v}) = m \\ \text{(b) } \psi(m; \boldsymbol{v}) \text{ is linear on the 2nd argument} \end{cases}$$

[2] [7] [13].

Consider (P; M; π; F; G), where P, M and F are differential varieties. π: the projection of P on M, a differential manifold. G: a diffeomorphism group from F to F. We will say that P is a fibered space of base M, of projection π, of fiber type F and of structural group G if:

i) $\forall m \in M$; $\pi^{-1}(m)$ is a manifold differentiable at F

ii) $\forall m \in M$; $\exists$ an open neighborhood U of m in M and a diffeomorphism $\psi: U * F \to \pi^{-1}(U)$

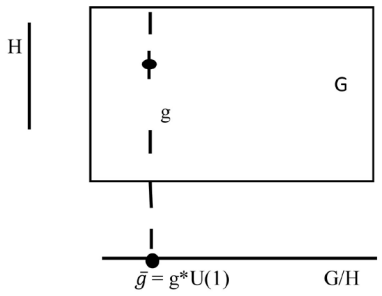

Figure 3. Fibration of G.

Such that $\begin{cases}\text{(a) } (\pi \text{ o } \psi)(m;v)=m \\ \text{(b) The applications } \psi_{\beta\alpha}=\psi_{\beta}^{-1} \text{ o } \psi_{\alpha}^{(m)} \text{ determine the elements of } G\end{cases}$

$(U; \psi)$ being called a local trivialization (Figure 4).

b) Definitions

Consider the point $P_o(1;0;0)$ of S^2, a point that we identify with the quaternion $i(0;1;0;0)$. The Hopf fibration h in terms of rotation is defined as below [1] [3]:

$$\begin{aligned} &h: S^3 \to S^2; q \to h(q)=R_q(i)=q*i*\bar{q} \\ &=\left(a^2+b^2-c^2-d^2;2(ad+bc);2(bd-ac)\right) \\ &=(x;y;z)=p; \text{ with } q=(a;b;c;d) \end{aligned} \tag{36}$$

1.3.3. Fiber over $P = (x; y; z)$ of S^2

Let us determine the fiber above a point $P(x;y;z)=p$ of S^2. In other words let us determine the set of points $Q=(a;b;c;d)=q$ of S^3 which verify $h(q) = p$; *i.e.* $h^{-1}(p)=q$ [1] and [3].

1) For $P_o(1;0;0)=i$; we have $h^{-1}(i)=(a;b;c;d)$ such that

$$\begin{cases} a^2+b^2-c^2-d^2=1 \\ ad+bc=0 \\ bd-ac=0 \end{cases}.$$

Hence $\begin{cases} a^2+b^2=1 \\ b=c=0 \end{cases}$. There are $\theta \in [0;2\pi] \cap R$ which checks $\begin{cases} a=\cos\theta \\ b=\sin\theta \end{cases}$

Thus

$$q=(a;b;c;d)=(\cos\theta;\sin\theta;0;0) \left(\text{or } q \equiv e^{i\theta}\right) \tag{37}$$

describes a circle of S^3.

2) For $P(-1;0;0)=-i$; we have $h^{-1}(-i)=(a;b;c;d)$ such that

$$\begin{cases} a^2+b^2-c^2-d^2=-1 \\ ad+bc=0 \\ bd-ac=0 \end{cases}.$$

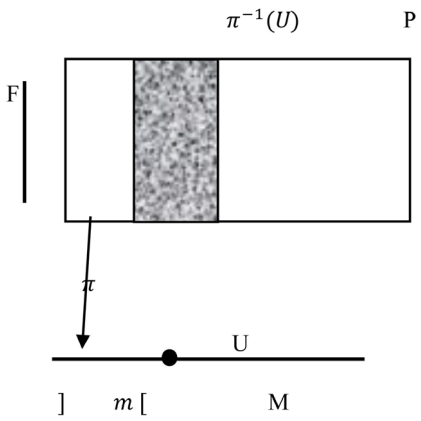

Figure 4. Fiber above the open U.

Hence $\begin{cases} c^2+d^2=1 \\ a=b=0 \end{cases}$. There are $\theta \in [0;2\pi] \cap R$ which checks $\begin{cases} c=\sin\theta \\ d=\cos\theta \end{cases}$

Thus

$$q=(a;b;c;d)=(0;0;\sin\theta;\cos\theta) \tag{38}$$

describes a circle S^3.

3) For $P(x;y;z)=p\in S^2\setminus\{(1;0;0);(-1;0;0)\}$. Let us look for q such that $R_1(i)=R_q(i)$. We then find $q=\left(\sqrt{\frac{1+x}{2}};0;\frac{-z}{\sqrt{2(1+x)}};\frac{y}{\sqrt{2(1+x)}}\right)$. Indeed; $\boldsymbol{OP}_o=(1;0;0)=i$, and $\boldsymbol{OP}=(x;y;z)$ such that $\boldsymbol{OP}_o\cdot\boldsymbol{OP}=\cos 2\theta=x$, by exploiting the relation (26); and $\boldsymbol{OP}_o \text{ л } \boldsymbol{OP}=i \text{ л } (xi+yj+zk)=-zj+yk$. Thus $\|\boldsymbol{OP}_o \text{ л } \boldsymbol{OP}\|=\|\boldsymbol{OP}_o\|\cdot\|\boldsymbol{OP}\|\cdot\sin 2\theta=\sin 2\theta$. We then find $\|\boldsymbol{OP}_o \text{ л } \boldsymbol{OP}\|=\sqrt{y^2+z^2}=\sqrt{1-x^2}$ because $x^2+y^2+z^2=1$. Thus $\cos\theta=\sqrt{\frac{1+x}{2}}$ and $\sin\theta=\sqrt{\frac{1-x}{2}}$. Consequently a following unit vector $\boldsymbol{OP}_o \text{ л } \boldsymbol{OP}$ is $\boldsymbol{u}=\frac{\boldsymbol{OP}_o \text{ л } \boldsymbol{OP}}{\|\boldsymbol{OP}_o \text{ л } \boldsymbol{OP}\|}=\frac{1}{\sqrt{1-x}}(-zj+yk)$. This unitary vector of axis of rotation, makes it possible to bring P_o in *P*. Consequently, according to (26), we finds $q=\cos\theta+\boldsymbol{u}\sin\theta$. We therefore have

$$q=\sqrt{\frac{1+x}{2}}+\frac{-zj+yk}{\sqrt{2(1+x)}}=\left(\sqrt{\frac{1+x}{2}};0;\frac{-z}{\sqrt{2(1+x)}};\frac{y}{\sqrt{2(1+x)}}\right) \tag{39}$$

The relation (37), allows us to affirm that the relation (39) is given by quaternions q describing a circle of S^3. Indeed; let q_1 and q_2 in S^3, such that $R_{q_1}(i)=R_{q_2}(i)=P(x;y;z)$.

From relation (23), it comes then that $R_{\overline{q_2}} \text{ o } R_{q_1}(i)=i=R_{\overline{q_2}*q_1}(i)$. And according to the relation (37), we obtain $\overline{q_2}*q_1=e^{i\theta}$; with $\theta\in[0;2\pi]$. We therefore deduce that

$$q_1=q_2*e^{i\theta};\ \text{with } \theta\in[0;2\pi], \tag{40}$$

describes a circle S^3.

1.3.4. Local Trivialization of Fibration *h*

The local trivialization of the *h* fibration is obtained from relations (39) and (40) below [1] [3]:

The fiber above $p(x;y;z)\in S^2$, is the circle parameterized by

$$\kappa:[0;2\pi]\to S^3;\beta\to\kappa(\beta)=q*e^{i\beta};\ \text{with } q=\frac{1}{\sqrt{2(1+x)}}\left((1+i)+yj+zk\right). \tag{41}$$

Indeed; from (9) we have $q=\cos\theta+p_1\sin\theta$ with $p_1\in\mathbb{H}_{pur}$. And from (26), *q* induces a rotation of angle 2θ, around the axis p_1. We can then study the rotation around $p(x;y;z)\in S^2$ as two rotations r_1 and r_2; bringing respec-

tively q in i, and i in p. In other words $R_q(i) = p = r_1 \circ r_2(q)$. The axis of this rotation is then the vector line perpendicular to the middle of the segment $P_o(1;0;0) = i$ and $P(x;y;z) = p$. This axis has the equation:

$$\boldsymbol{w} = (i + xi + yj + zk)/2 = ((1+x)i + yj + zk)/2$$

We find that $\|\boldsymbol{w}\| = \frac{1}{2}\sqrt{(1+x)^2 + y^2 + z^2} = \frac{1}{2}\sqrt{2(1+x)}$ because $x^2 + y^2 + z^2 = 1$. We have $\|\boldsymbol{w}\| = \sqrt{\frac{1+x}{2}}$. Consequently the unit vector, along this axis, is $\boldsymbol{u} = \frac{\boldsymbol{w}}{\|\boldsymbol{w}\|} = \sqrt{\frac{2}{1+x}}\left[\frac{(1+x)i + yj + zk}{2}\right]$.

Thus $\boldsymbol{u} = \sqrt{\frac{1}{2(1+x)}}((1+x)i + yj + zk)$. Consequently

$q = \frac{1}{\sqrt{2(1+x)}}((1+x)i + yj + zk) = \boldsymbol{u}$, which give

$$q = \cos(\pi/2) + [\sin(\pi/2)]([(1+x)i + yj + zk])/|(1+x)i + yj + zk|;$$

which is a quaternion of the fiber above p. And according to (40), this fiber is of the form $\{q * e^{i\beta}\}$ with $\beta \in [0;2\pi] \cap R$.

Therefore the application

$$\psi : U * S^1 \to S^3 \setminus h^{-1}(-i), ((x;y;z);e^{i\beta}) \to \frac{(1+x)i + yj + zk}{\sqrt{2(1+x)}} * e^{i\beta}; \quad (42)$$

allows us to obtain local trivialization (U; ψ).

1.4. Stereographic Projection Visualizing the Fibration of HOPF from the Lie *SU*(2) Group

Stereographic projection is a method of representing a sphere, deprived of a point, on a plane. [1] [3] [5] [7] [8] [12].

The relation (13) gives us

$$\psi_{N'} : U_{N'} \to \mathbb{R}^2, \text{ with } \psi_{N'}(x,y,z) = (x/(1-z), y/(1-z)) \quad (43)$$

presents the stereographic projection. This sends the point $P(x;y;z)$, from $S^2 \setminus \{(0;0;1)\}$, is sent in P' from the plane Π = Γ. Straight line NP cut Π in P' (**Figure 5**).

A circle of S^2 which passes through the north pole $N(0;0;1)$; being in a plane Γ', is sent by $\psi_{N'}$ to the intersection line of Γ and Γ'.

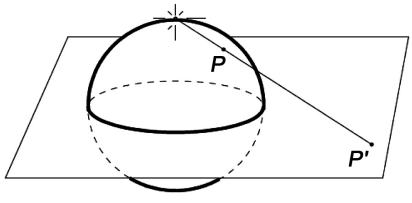

Figure 5. Stereographic projection of the north pole on a non-equatorial plane [1].

A circle of S^2 which does not pass through the north pole *N*, is projected into a circle of Γ by $\psi_{N'}$.

The generalization of stereographic projection to all dimensions being possible, let us take again the relation (15). He comes

$$\begin{aligned} &\varphi_N : U_N = S^3 \setminus \{(0,0,0;1)\} \to \mathbb{R}^3, \\ &\text{with } \varphi_N(a,b,c,d) = \left(b/(1-a), c/(1-a), d/(1-a)\right) \end{aligned} \tag{44}$$

Let us determine the images of the fibers above the elements of S^2, by means of this stereographic projection φ_N. We find

1)

$$\begin{aligned} \varphi_N \circ h^{-1}(P_0) &= \varphi_N \circ h^{-1}(i) = \varphi_N \circ h^{-1}((1;0;0)) = \varphi_N\left[h^{-1}(i)\right] \\ &= \varphi_N\left[(\cos\theta;\sin\theta;0;0)\right] \ (\text{from relation } (37)) \\ &= \left(\frac{\sin\theta}{1-\cos\theta},0,0\right) = \left(\frac{\cos\frac{\theta}{2}}{\sin\frac{\theta}{2}},0,0\right) = \left(\cot\frac{\theta}{2},0,0\right) \end{aligned} \tag{45}$$

which is the *x*-axis of the plane (*x*, *y*) or (*x*, *z*) of $\mathbb{R}^3 = (x;y;z)$; that is to say a circle of infinite radius.

2)

$$\begin{aligned} \varphi_N \circ h^{-1}(P) &= \varphi_N \circ h^{-1}(-i) = \varphi_N \circ h^{-1}((-1;0;0)) = \varphi_N\left[h^{-1}(-i)\right] \\ &= \varphi_N\left[(0;0;\sin\theta;\cos\theta)\right] \ (\text{from relation } (38)) \\ &= (0;\sin\theta;\cos\theta) \end{aligned} \tag{46}$$

which is a circle of the plane (*y*, *z*) of $\mathbb{R}^3 = (x;y;z)$.

3)

$$\begin{aligned} &\varphi_N \circ h^{-1}(P) = \varphi_N \circ h^{-1}(p(x;y;z)) \\ &= \varphi_N\left(\left(\cos\theta;0;\frac{-z*\sin\theta}{\sqrt{1-x^2}};\frac{y*\sin\theta}{\sqrt{1-x^2}}\right)\right) \ (\text{from relation } (39)) \\ &= \left(0;\frac{-z*\sin\theta}{(1-\cos\theta)*\sqrt{1-x^2}};\frac{y*\sin\theta}{(1-\cos\theta)*\sqrt{1-x^2}}\right) \\ &\text{with } \begin{cases} \cos\theta = \sqrt{\frac{1+x}{2}} \\ \sin\theta = \sqrt{\frac{1-x}{2}} \end{cases} = \left(0;\frac{-z*\cot\frac{\theta}{2}}{\sqrt{1-x^2}};\frac{y*\cot\frac{\theta}{2}}{\sqrt{1-x^2}}\right) \end{aligned} \tag{47}$$

and according to the relation (40) is a circle of space $\mathbb{R}^3 = (x;y;z)$.

These different images of the circles, by stereographic projection φ_N, give circles which are linked in chains like those of the Olympic games (**Figure 6**).

1.5. Heat Transfer Equation

1.5.1. Transport Phenomena

1) What do we mean by transport phenomenon?

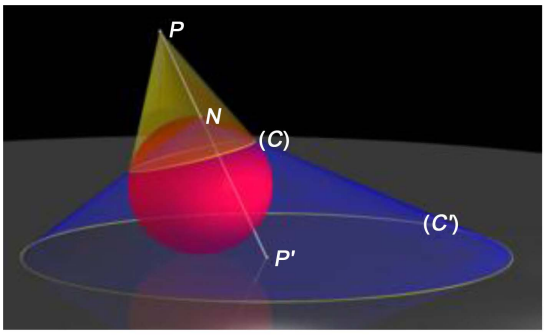

Figure 6. The stereographic projection transforms the circles of the sphere into circles of the projection plane [7] [8].

In thermo-statistics, we group together a set of physical phenomena of movement of molecules in fluids or solids in transport phenomena. Transport phenomena are the processes in which there is a global transfer (or transport) of matter, energy or momentum on a macroscopic scale. The essential physical aspects of these phenomena can be described by similar methods and are characterized by an equation which links the variation in time and in space of a quantity which describes the phenomenon. In the simplest case this equation is of the form [14] [15] [16] [17]:

$$\frac{\partial \xi}{\partial t} = a^2 \frac{\partial^2 \xi}{\partial x^2} \tag{48}$$

where a is a constant characteristic of each physical situation and ξ is a quantity corresponding to the particular phenomenon of transport studied like the diffusion of the molecules, the viscosity and the conduction of heat. In this work, we will focus on the last case of these types of transport phenomena whose mathematical solutions relate to a temperature distribution.

The phenomenon of energy and/or material transport is of great importance in statistical physics. This phenomenon for heat is described by the Fourier equation which we will solve for a spatial dimension before modeling this solution for the Kankule site. The solution of this equation is called the geotherm

2) One-dimensional Fourier equation

The Fourier equation for the conduction of heat in the ground, when this energy varies as a function of time t and depth z is:

$$\frac{\partial^2 T}{\partial z^2} - \frac{1}{\alpha}\frac{\partial T}{\partial t} = 0 \tag{49}$$

[5] [14] [15] [16] [18] [19] [20] [21] [22].

With α the coefficient of thermal diffusivity of the soil, z the depth and T the temperature characterizing the heat transported.

With the boundary conditions of the first species (Dirichlet problem), where the surface temperature is known at all times, this equation admits a sinusoidal solution of progressive wave of the form:

$$T(z,t) = \mathrm{e}^{i(kz-\omega t)} \tag{50}$$

whose

ω : is the pulsation of the waves

$\frac{\omega}{k} = v$: is the phase velocity of these waves

i: the imaginary unit (with $i^2 = -1$)

Introduce the values of (50) in (49), we find:

$$-k^2 + i\frac{\omega}{\alpha} = 0 \tag{51}$$

So,

$$\omega = i\alpha k^2 \tag{52}$$

As a result

$$k = \pm(1+i)\sqrt{\frac{\omega}{2\alpha}} \tag{53}$$

is

$$k = \frac{\pm(1+i)}{d} \tag{54}$$

by asking

$$d = \sqrt{\frac{2\alpha}{\omega}} \tag{55}$$

d: is called the depth of penetration of the waves (or also the depth of damping).

Starting from (49), according to Wu and Nofziger [22], taking into account the boundary conditions, the previous solution can be written:

$$T(z,t) = \overline{T_0} + \overline{A_0} \cdot \mathrm{e}^{-\frac{z}{d}} \sin\left(\frac{2\pi(t-t_0)}{365} - \frac{z}{d} - \frac{\pi}{2}\right) \tag{56}$$

Using solution of (49), we looked for the gradient, for each site, with the relation $\partial T/\partial z = f(z)$ and deduce the depth of exploration to the Kankule site studies

3) Exploitation of geothermy

The Geoscience review of March 16, 2013, shows the operating conditions of geothermal energy to produce electricity. Having active tectonic or volcanic zones in which a surface heat source makes it possible to have a geothermal fluid at a temperature sufficient to produce electricity [23]. On page 14, Figure 8 [23], already shows that with a temperature of 50˚C at 1 km deep, we can consider the production of electricity. It will then be necessary to dig for this to more than 3 km deep, in order to trap the geothermal fluid at more than 150˚C. The same article presents a world map where high energy geothermal energy is likely to be exploited. Eastern DR. Congo is there, as in all the countries of the Albertine Rift (or Valley). From the ground temperature down to 90˚C, electricity can already be produced [24].

The latest study distinguishes between surface and deep geothermal energy as follows:

- <30˚C and <500 m: surface geothermal energy. This takes up the very low temperatures (enthalpy).
- between 25˚C - 30˚C and 150˚C and >500 m: deep geothermal energy. This takes over the low and medium temperatures (enthalpy).

Still the same study, specifies that if the geothermal reservoir reaches a temperature above 150˚C and is encountered at shallow depths, the resource must therefore be in a region where the geothermal gradient is normal (~30˚C/km) or beyond normal. This is for the production of electricity. This classification is consistent with that suggested by Lindal for France [25].

The exploitation of high energy geothermal energy is favorable in areas which knows geodynamic contexts, showing some form of volcanism. At these points, a significant part of the internal energy of the globe is released. The history of mountain chain formations and terrestrial magmatism allows us to understand the genesis of magma chambers. The latter are foci, zones with strong thermal gradient [26].

1.5.2. Hopf Fiber of the Heat Transfer Phenomenon

Relations (50) or (56) determine solutions of Equation (49).

Take

$$q = \frac{T(z,t)}{|T(z,t)|} = (\cos\theta; \sin\theta; 0; 0); \text{ with } \theta = (\pm z/d - \omega t) \in [0; 2\pi] \cap R \quad (57)$$

By comparing to relation (38), we observe that q is a fiber above the north pole. Our q being a solution of (50) or (56); we conclude that each solution of these equations is associated with a fiber in $SU(2) = S^3$.

For the three-dimensional Fourier equation

$$\frac{\partial T}{\partial t} = \alpha \Delta T; \text{ with } \Delta = \frac{\partial^2}{\partial x^2} + \frac{\partial^2}{\partial y^2} + \frac{\partial^2}{\partial xz^2} \quad (58)$$

the Laplacian; there is always a quaternion of the type (56) which is a solution; by means of a modification of x by a three-dimensional vector. In short, there is always a quaternion unit, which is a fiber. From the above, we conclude that for each solution of the Fourier heat transfer equation, there is an associated fiber in $SU(2) = S^3$. This result is analogous to what in classical electromagnetism is called magnetic field lines. What we can visualize as below (**Figure 7**).

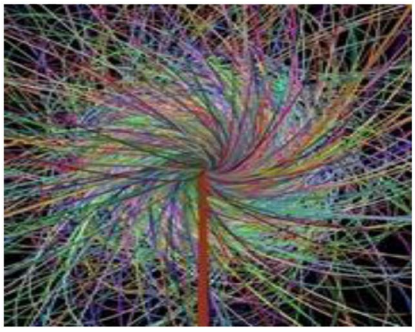

Figure 7. Model of a heat fiber [7] [12].

This model is analogous to that obtained by T.M. and Dirk Bouwmeester [27], for the modeling of lights (electromagnetic waves of the visible spectrum) with Hopf fibration. Indeed, each fiber appears as a line of Earth's magnetic field. And since two distinct lines of fields don't join, so do two fibers in circles that don't cut. And since two distinct lines of fields don't join, so do two fibers in circles that don't cut. As a result each geomagnetic field line is representative of a heat fiber. By exploiting Maxwell's equations of the Terrestrial geomagnetic field, we find that

$$B = B_0 * \mathrm{e}^{-k_1 x} \mathrm{e}^{i\left(k_2 x - \varpi t\right)} \quad [28], \tag{59}$$

which is a solution of the same type as (50).

2. Methodology

To do this work, we used the following methodological approach:

2.1. Analytic

To do this we sought:

- Let us relate it between Quaternions units and the Lie group $SU(2)$;
- determining the coefficients of the geotherm;
- The links between the Geotherm of the one-dimensional Fourier equation with the Hopf fibration of the sphere S^3;
- See how to visualize Hopf fibration using stereographic projection;
- The significance in terms of bundle of the geotherm.

2.2. Experimental

1) From 8 h to 14 h, with the ground thermometer, we took samples from 14 sites, called Kankule I, Kankule II,…, and Kankule XIV:

We took soil temperatures up to 15 centimeters deep, every day, in 52 weeks. This in order to characterize each site by the average temperature of the surface soil;

Also took the temperatures of the thermal waters, over the same period from September 2010 to December 2014, in order to see how to also differentiate the sites from the electrolytic properties of its waters. The analysis of which was carried out at the Lwiro Natural Sciences Research Center (CNRS/Lwiro) in Katana.

2) With a Garmin brand GPS, we determined the geographic coordinates of each site. Using these coordinates we had:

- Geo referenced each site
- Downloaded on the NOAA site, the geomagnetic fields of each site, for the same years of our temperature samples [29].

2.3. Comparative

To do this, we compared our results from the ground geotherm with various accepted results, in order to see if each thermal source can be compared to a bundle.

2.4. Statistical

Using statistics we were able to:

- Determine different coefficients involved in the geotherm of each site.
- Perform the linear regression of the geomagnetic field for each site according to the temperature field of the same site.

3. Results and Analysis

1) Our study rather leads to the result:

$$T(z,t)=\overline{T_0}+\overline{A_0}\cdot \mathrm{e}^{-\frac{z}{d}}\sin\left(\frac{2\pi(t-t_0)}{365}-\frac{z}{d}+\frac{3\pi}{4}\right) \tag{60}$$

as solution of Equation (49).

Indeed, consider the depreciated waves real parts of the solution (50), which are $U_1(z,t)=\mathrm{e}^{-\frac{z}{d}}\cos\left(\omega t-\frac{z}{d}\right)$ and $U_2(z,t)=\mathrm{e}^{-\frac{z}{d}}\sin\left(-\omega t+\frac{z}{d}\right)$. Superposing the two waves, we find the solution:

$$\begin{aligned}
U_3(z,t)&=U_1(z,t)+U_2(z,t)\\
&=\mathrm{e}^{-\frac{z}{d}}\cos\left(\omega t-\frac{z}{d}\right)+\mathrm{e}^{-\frac{z}{d}}\sin\left(-\omega t+\frac{z}{d}\right)\\
&=\mathrm{e}^{-\frac{z}{d}}\left(\cos\left(\omega t-\frac{z}{d}\right)+\sin\left(-\omega t+\frac{z}{d}\right)\right)\\
&=\mathrm{e}^{-\frac{z}{d}}\left[\cos\left(\omega t-\frac{z}{d}\right)-\sin\left(\omega t-\frac{z}{d}\right)\right]\\
&=\mathrm{e}^{-\frac{z}{d}}\left[\cos\left(\omega t-\frac{z}{d}\right)-\cos\left(\frac{\pi}{2}-\left(\omega t-\frac{z}{d}\right)\right)\right]\\
&=\mathrm{e}^{-\frac{z}{d}}\left[-2\sin\left(\frac{\omega t-\frac{z}{d}+\frac{\pi}{2}-\omega t+\frac{z}{d}}{2}\right)*\sin\left(\frac{\omega t-\frac{z}{d}+\frac{\pi}{2}-\omega t+\frac{z}{d}}{2}\right)\right]\\
&=\mathrm{e}^{-\frac{z}{d}}\left[-2\sin\left(\frac{\pi}{4}\right)*\sin\left(\omega t-\frac{z}{d}-\frac{\pi}{4}\right)\right]\\
&=\mathrm{e}^{-\frac{z}{d}}\left[-2\frac{\sqrt{2}}{2}*\sin\left(\omega t-\frac{z}{d}-\frac{\pi}{4}\right)\right]\\
&=\sqrt{2}\mathrm{e}^{-\frac{z}{d}}\sin\left(\pi+\omega t-\frac{z}{d}-\frac{\pi}{4}\right)\\
&=\sqrt{2}\mathrm{e}^{-\frac{z}{d}}\sin\left(\omega t-\frac{z}{d}+\frac{3\pi}{4}\right)
\end{aligned}$$

Multiplying $U_3(z,t)$ by a real constant A, we still get a solution $U_4(z,t)=A*U_3(z,t)$ of Equation (49). By posing $\overline{A_0}=A*\sqrt{2}$, then we write $U_4(z,t)=\overline{A_0}*\mathrm{e}^{-\frac{z}{d}}\sin\left(\omega t-\frac{z}{d}+\frac{3\pi}{4}\right)$. We have a particular solution of (49) which is $U_5(0,t)=\overline{T_0}$, with $\overline{T_0}$ a real constant. Finally by supposing the waves

$U_4(z,t)$ and $U_5(0,t)$, we get the solution (60). In other words, we have:

$$T(z,t)=U_5(0,t)+U_4(z,t)=\overline{T_0}+\overline{A_0}\cdot e^{-\frac{z}{d}}\sin\left(\frac{2\pi(t-t_0)}{365}-\frac{z}{d}+\frac{3\pi}{4}\right)$$

Using statistical methods, we obtained, for each Kankule site, the coefficients of the geotherm (56) or ((56)-bis) given by Table 1.

2) By seeking the linear regression of the geomagnetic field B, expressed in micron-tesla, as a function of the temperature field T of the soil, expressed in degrees Celsius, we have obtained the relation of the type $B = aT + b$. The results of this regression are summarized in Table 2.

In this table, Ho is the null hypothesis. It translates the acceptance of the linear dependence between B and T. On each column, where Ho appears, the value 1 means acceptance of the null hypothesis. On the other hand the value 0, implies the rejection of the null hypothesis.

In order to better understand whether each site should be considered separately, we have analyzed which ions are found in different thermal waters, per site. Table 3 gives us a summary of the results found.

3) The geotherm (60) gives us the gradient

$$\text{grad}(z,t)=-\sqrt{2}\frac{A_0}{d}e^{-\frac{z}{d}}\cos\left(\frac{2\pi(t-t_0)}{365}--\frac{z}{d}+\frac{\pi}{2}\right) \quad (61)$$

Is $g(z)=\frac{\partial T}{\partial z}=-\frac{A_0}{z}e^{-\frac{z}{d}}\sin\left[\frac{2\pi(t-t_0)}{365}-\frac{z}{d}+\frac{3\pi}{4}\right]$ $-\frac{A_0}{z}e^{-\frac{z}{d}}\cos\left[\frac{2\pi(t-t_0)}{365}-\frac{z}{d}+\frac{3\pi}{4}\right]$ a function that varies with depth z.

Table 1. The coefficients of the geotherm by Kankule thermal spring.

Sites	A_0	T_0	D	α	σ
KANKULE I	13.5	23.88333	1.5600934	0.0000024	3.9105
KANKULE II	7.2	21.56666	0.6734899	0.0000005	1.688189
KANKULE III	6	21.5083333	0.7197964	0.0000005	1.804262
KANKULE IV	10.9	22.266666	1.0212474	0.000001	2.559888
KANKULE V	21.3	24.391666	1.9056126	0.0000036	4.776662
KANKULE VI	9.1	23.1833333	1.2840186	0.0000016	3.218557
KANKULE VII	26.5	21.15	2.6853818	0.0000072	6.731254
KANKULE VIII	24	22.7583333	2.1953011	0.0000048	5.502804
KANKULE IX	33.5	21.5916666	3.2440723	0.0000105	8.131683
KANKULE X	22.2	24.3916666	1.9716666	0.0000039	4.943021
KANKULE XI	15.4	24.85	1.3300099	0.0000018	3.333841
KANKULE XII	23.8	26.6416666	2.5989733	0.0000067	6.51466
KANKULE XIII	21.6	24.7583333	2.6707744	0.0000071	6.694639
KANKULE XIV	26.1	26.3583333	2.1395155	0.0000046	5.36297

An array where the coefficients of the two parallel lines differ.

Table 2. Reduction of the magnetic field B as a function of the soil temperature.

	A	B	Ho 0.001	Ho 0.01	Ho 0.05	Grad max
Kankule I	5.196e−02	4.964e−15	1	1	1	0.09419068
Kankule II	3.888e−01	−2.561e−14	1	0	0	0.12567529
Kankule III	5.017e−01	−6.483e−14	0	0	0	0.09799187
Kankule IV	4.610e−01	−5.989e−14	0	0	0	0.1254712
Kankule V	2.117e−01	6.208e−15	1	1	1	0.13139944
Kankule VI	1.917e−03	2.475e−16	1	1	1	0.08331411
Kankule VII	2.438e−01	8.349e−15	1	1	1	0.11600811
Kankule VIII	2.049e−01	6.800e−15	1	1	1	0.1285185
Kankule IX	2.932e−01	9.414e−15	1	1	0	0.12139556
Kankule X	3.176e−01	−9.710e−15	1	1	0	0.13234238
Kankule XI	2.495e−01	−2.501e−14	1	1	1	0.136118
Kankule XII	4.278e−01	−4.870e−14	1	0	0	0.10765238
Kankule XIII	3.515e−01	2.281e−14	1	1	0	0.09507472
Kankule XIV	−1.140e−01	−1.060e−14	1	1	1	0.143408

Table 3. Thermal water electrolysis data and associated thermal field.

Sites	T_sol	T_eau	Champ B	Cl^- (mg/L)	SO_4^- (mg/L)	HCO_3^- (mg/L)	PO_4^- (µmole/L)	NH_4^+ (µmole/L)	NO_3^- (µmole/L)
Kank I	29.817	54.3096	33.05609	7	492	322.5	0.133	76.5	5.1
Kank II	22.74	54.3625	33.05585	6.4	484.32	330	0.071	44.2	8.5
Kank III	22.54	45.3692	33.05509	6.3	539.52	310	0.062	28.9	34
Kank IV	26.031	66.2077	33.05529	6.3	460.8	360	0.111	28.9	32.3
Kank V	36.012	62.9192	33.05565	7.1	542.4	337.5	0.071	137.7	18.7
Kank VI	27.45	47.6058	33.05584	7	537.12	350	0.093	54.4	18.7
Kank VII	39.46	64.1539	33.05584	7.25	549.6	335	0.084	49.3	45.9
Kank VIII	31.898	50.701	33.05574	7	540	347.5	0.089	96.9	11.9
Kank IX	31.335	64.1885	33.05604	8	520.8	321	0.089	64.6	17
Kank X	35.923	63.8846	33.05599	7.1	497.28	347.5	0.097	34	18.7
Kank XI	35.231	69.8817	33.05592	6.8	508.8	352.5	0.093	102	15.3
Kank XII	37.006	64.9212	33.05557	6.1	530.4	300	0.111	64.6	6.8
Kank XIII	37.81	63.3144	33.05539	6.5	528	298	0.111	105.4	20.4
Kank XIV	41.49	62.5039	33.05609	5.5	508.8	285	0.129	71.4	51

Let's determine the maximum values of this function, using differential calculus. It comes at a given depth

$$\begin{cases} g(z)>0 \\ g'(z)=0 \\ g''(z)<0 \end{cases}$$

$$\Leftrightarrow \begin{cases} -\frac{A_0}{z}\mathrm{e}^{-\frac{z}{d}}\left(\sin\left[\frac{2\pi(t-t_0)}{365}-\frac{z}{d}+\frac{3\pi}{4}\right]+\mathrm{e}^{-\frac{z}{d}}\cos\left[\frac{2\pi(t-t_0)}{365}-\frac{z}{d}+\frac{3\pi}{4}\right]\right)>0 \\ 2\frac{A_0}{d^2}\mathrm{e}^{-\frac{z}{d}}\cos\left[\frac{2\pi(t-t_0)}{365}-\frac{z}{d}+\frac{3\pi}{4}\right]=0 \\ 2\frac{A_0}{d^3}\mathrm{e}^{-\frac{z}{d}}\left(\sin\left[\frac{2\pi(t-t_0)}{365}-\frac{z}{d}+\frac{3\pi}{4}\right]-\cos\left[\frac{2\pi(t-t_0)}{365}-\frac{z}{d}+\frac{3\pi}{4}\right]\right)<0 \end{cases}$$

$$\Leftrightarrow \begin{cases} g(z)=\frac{A_0}{z}\mathrm{e}^{-\frac{z}{d}}>0 \\ \frac{2\pi(t-t_0)}{365}-\frac{z}{d}+\frac{3\pi}{4}=(2k+1)\frac{\pi}{2};\ \text{with } k\in\mathbb{Z} \\ \sin(2k+1)\frac{\pi}{2}<0 \end{cases} \tag{62}$$

With $\frac{z}{d}>0$, the first value of z which makes the gradient maximum, is obtained for $k=-1$.

We then find the following results for the Kankule IV site:

(Abscissa of the maximum) $z=d*\pi(1.25+60/365)=4.537828208$ m and the maximum gradient

$$g(z)=\partial T/\partial z=0.125471195^{\circ}\mathrm{C/m} \tag{63}$$

For all site of Kankule the average maxima gradient give

$$\bar{m}=0.117[^{\circ}\mathrm{C/m}] \tag{64}$$

4. Discussion of the Results

4.1. Which of the Geotherms (56) and (60) Verify (49)?

To find out, we then introduce these results into Equation (49) and see more.

For Equation (49) for which Wu and Nofziger find the solution.

$$T=T(z,t)=T_a+A_0\mathrm{e}^{-\frac{z}{d}}\sin\left[\frac{2\pi(t-t_0)}{365}-\frac{z}{d}-\frac{\pi}{2}\right],$$

with $d=\sqrt{\frac{2\alpha}{\omega}}$ and $\omega=2\pi/365$.

He then comes

1)

$$\begin{aligned} T_t'(z;t)&=\frac{1}{\alpha}\frac{\partial T}{\partial t}=\frac{1}{\alpha}\frac{2\pi}{365}A_0\mathrm{e}^{-\frac{z}{d}}\cos\left[\frac{2\pi(t-t_0)}{365}-\frac{z}{d}-\frac{\pi}{2}\right] \\ &=\frac{A_0}{\alpha}\omega\mathrm{e}^{-\frac{z}{d}}\cos\left[\frac{2\pi(t-t_0)}{365}-\frac{z}{d}-\frac{\pi}{2}\right] \end{aligned} \tag{65}$$

2)

$$T_z''(z;t)=\frac{\partial^2 T}{\partial z^2}=\frac{\partial}{\partial z}\left(\frac{\partial T}{\partial z}\right)$$

$$=\frac{\partial}{\partial z}\left[-\frac{A_0}{d}\mathrm{e}^{-\frac{z}{d}}\sin\left(\frac{2\pi(t-t_0)}{365}-\frac{z}{d}-\frac{\pi}{2}\right)-\frac{A_0}{d}\mathrm{e}^{-\frac{z}{d}}\cos\left(\frac{2\pi(t-t_0)}{365}-\frac{z}{d}-\frac{\pi}{2}\right)\right]$$

$$=-\frac{A_0}{d}\frac{\partial}{\partial z}\left[\mathrm{e}^{-\frac{z}{d}}\left(\cos\left(\frac{2\pi(t-t_0)}{365}-\frac{z}{d}-\frac{\pi}{2}\right)-\cos\left(\frac{2\pi(t-t_0)}{365}-\frac{z}{d}\right)\right)\right]$$

$$=\frac{2A_0}{d}\frac{\partial}{\partial z}\left[\mathrm{e}^{-\frac{z}{d}}\sin\left(\frac{2\pi(t-t_0)}{365}-\frac{z}{d}-\frac{\pi}{4}\right)\sin\left(-\frac{\pi}{4}\right)\right]$$

$$=-\frac{\sqrt{2}}{d}A_0\frac{\partial}{\partial z}\left[\mathrm{e}^{-\frac{z}{d}}\sin\left(\frac{2\pi(t-t_0)}{365}-\frac{z}{d}-\frac{\pi}{4}\right)\right]$$

$$=-\frac{\sqrt{2}}{d}A_0\left[-\frac{1}{d}\mathrm{e}^{-\frac{z}{d}}\sin\left(\frac{2\pi(t-t_0)}{365}-\frac{z}{d}-\frac{\pi}{4}\right)-\frac{1}{d}\mathrm{e}^{-\frac{z}{d}}\cos\left(\frac{2\pi(t-t_0)}{365}-\frac{z}{d}-\frac{\pi}{4}\right)\right]$$

$$=\frac{\sqrt{2}}{d^2}A_0\mathrm{e}^{-\frac{z}{d}}\left[\sin\left(\frac{2\pi(t-t_0)}{365}-\frac{z}{d}-\frac{\pi}{4}\right)+\cos\left(\frac{2\pi(t-t_0)}{365}-\frac{z}{d}-\frac{\pi}{4}\right)\right]$$

$$=\frac{\sqrt{2}}{d^2}A_0\mathrm{e}^{-\frac{z}{d}}\left[\sin\left(\frac{2\pi(t-t_0)}{365}-\frac{z}{d}-\frac{\pi}{4}\right)+\sin\left(\frac{2\pi(t-t_0)}{365}-\frac{z}{d}-\frac{\pi}{4}+\frac{2\pi}{4}\right)\right] \quad (66)$$

$$=\frac{\sqrt{2}}{d^2}A_0\mathrm{e}^{-\frac{z}{d}}\left[\sin\left(\frac{2\pi(t-t_0)}{365}-\frac{z}{d}-\frac{\pi}{4}\right)+\sin\left(\frac{2\pi(t-t_0)}{365}-\frac{z}{d}+\frac{\pi}{4}\right)\right]$$

$$=\frac{2}{d^2}A_0\mathrm{e}^{-\frac{z}{d}}\sin\left(\frac{2\pi(t-t_0)}{365}-\frac{z}{d}\right)=\frac{A_0}{\alpha}\omega\mathrm{e}^{-\frac{z}{d}}\sin\left[\frac{2\pi(t-t_0)}{365}-\frac{z}{d}\right]$$

Comparing solutions (65) and (66), we find that the two results differ. We then conclude that solution (56), given by Wu and Nofziger is not suitable as solution of (49).

The result (60) that we found for the geotherm being

$$T=T(z,t)=T_a+A_0\mathrm{e}^{-\frac{z}{d}}\sin\left[\frac{2\pi(t-t_0)}{365}-\frac{z}{d}+\frac{3\pi}{4}\right],$$

with $d=\sqrt{\frac{2\alpha}{\omega}}$ and $\omega=\frac{2\pi}{365}$.

Then he comes:

1)

$$T_t'(z;t)=\frac{1}{\alpha}\frac{\partial T}{\partial t}=\frac{1}{\alpha}\frac{2\pi}{365}A_0\mathrm{e}^{-\frac{z}{d}}\cos\left[\frac{2\pi(t-t_0)}{365}-\frac{z}{d}+\frac{3\pi}{4}\right]$$
$$=\frac{A_0}{\alpha}\omega\mathrm{e}^{-\frac{z}{d}}\cos\left[\frac{2\pi(t-t_0)}{365}-\frac{z}{d}+\frac{3\pi}{4}\right] \quad (67)$$

2)

$$
\begin{aligned}
T_z''(z;t) &= \frac{\partial^2 T}{\partial z^2} = \frac{\partial}{\partial z}\left(\frac{\partial T}{\partial z}\right) \\
&= \frac{\partial}{\partial z}\left[-\frac{A_0}{d}\mathrm{e}^{-\frac{z}{d}}\sin\left(\frac{2\pi(t-t_0)}{365}-\frac{z}{d}+\frac{3\pi}{4}\right)-\frac{A_0}{d}\mathrm{e}^{-\frac{z}{d}}\cos\left(\frac{2\pi(t-t_0)}{365}-\frac{z}{d}+\frac{3\pi}{4}\right)\right] \\
&= -\frac{A_0}{d}\frac{\partial}{\partial z}\left[\mathrm{e}^{-\frac{z}{d}}\left(\sin\left(\frac{2\pi(t-t_0)}{365}-\frac{z}{d}+\frac{3\pi}{4}\right)+\sin\left(\frac{2\pi(t-t_0)}{365}-\frac{z}{d}+\frac{3\pi}{4}+\frac{2\pi}{4}\right)\right)\right] \\
&= -\frac{2A_0}{d}\frac{\partial}{\partial z}\left[\mathrm{e}^{-\frac{z}{d}}\sin\left(\frac{2\pi(t-t_0)}{365}-\frac{z}{d}+\frac{3\pi}{4}+\frac{\pi}{4}\right)\cos\left(\frac{\pi}{4}\right)\right] \\
&= -\frac{\sqrt{2}}{d}A_0\frac{\partial}{\partial z}\left[\mathrm{e}^{-\frac{z}{d}}\sin\left(\frac{2\pi(t-t_0)}{365}-\frac{z}{d}+\pi\right)\right] \\
&= \frac{\sqrt{2}}{d}A_0\frac{\partial}{\partial z}\left[\mathrm{e}^{-\frac{z}{d}}\sin\left(\frac{2\pi(t-t_0)}{365}-\frac{z}{d}\right)\right] \\
&= \frac{\sqrt{2}}{d}A_0\left[-\frac{1}{d}\mathrm{e}^{-\frac{z}{d}}\sin\left(\frac{2\pi(t-t_0)}{365}-\frac{z}{d}\right)-\frac{1}{d}\mathrm{e}^{-\frac{z}{d}}\cos\left(\frac{2\pi(t-t_0)}{365}-\frac{z}{d}\right)\right] \\
&= -\frac{\sqrt{2}}{d^2}A_0\mathrm{e}^{-\frac{z}{d}}\left[\sin\left(\frac{2\pi(t-t_0)}{365}-\frac{z}{d}\right)+\sin\left(\frac{2\pi(t-t_0)}{365}-\frac{z}{d}+\frac{\pi}{2}\right)\right] \\
&= -\frac{\sqrt{2}}{d^2}A_0\mathrm{e}^{-\frac{z}{d}}\left[2\sin\left(\frac{2\pi(t-t_0)}{365}-\frac{z}{d}+\frac{\pi}{4}\right)\cos\left(-\frac{\pi}{4}\right)\right] \\
&= -\frac{2}{d^2}A_0\mathrm{e}^{-\frac{z}{d}}\sin\left(\frac{2\pi(t-t_0)}{365}-\frac{z}{d}+\frac{\pi}{4}\right) \\
&= -\frac{A_0}{\alpha}\omega\mathrm{e}^{-\frac{z}{d}}\sin\left[\frac{2\pi(t-t_0)}{365}-\frac{z}{d}+\frac{\pi}{4}\right] \\
&= \frac{A_0}{\alpha}\omega\mathrm{e}^{-\frac{z}{d}}\cos\left[\frac{2\pi(t-t_0)}{365}-\frac{z}{d}+\frac{\pi}{4}+\frac{2\pi}{4}\right]
\end{aligned}
\tag{68}
$$

Comparing solutions (67) and (68), we find that the two results are equal. We then conclude that the relation (60), is suitable as solution of (49).

This analysis of the solution used by Wu and Nofziger shows that it is not the integral of the one-dimensional Fourier Equation (49). This is why it has not been exploited by Alonso/Finn [15]. The result of the latter verifies the Fourier equation. Its only problem is that some constants of the geotheme are not well specified

4.2. Does Each Thermal Water Site Represent a Bundle?

As a result, the geotherm (50) takes the form: $T(z,t)=\mathrm{e}^{i\left(\pm\left(\frac{1+i}{d}\right)z-\omega t\right)}$; a quaternion of module $\left|T(z,t)\right|=\begin{cases}\mathrm{e}^{\frac{-z}{d}}\\ \mathrm{e}^{\frac{z}{d}}\end{cases}$.

The solutions which have a physical meaning are those for which $\left|T(z,t)\right|=\mathrm{e}^{\frac{-z}{d}}$, corresponding to the propagation of the heat-absorbed waves.

Always starting from (50), we get the following real solution for (60):

$$T(z,t)=\overline{T_0}+\overline{A_0}\mathrm{e}^{-\frac{z}{d}}\sin\left(\frac{2\pi(t-t_0)}{365}-\frac{z}{d}+\frac{3\pi}{4}\right)$$

Result called integral curve of (49) or geothermal. It is this result that Adelin MULENDA [1] applies for the Kankule site.

If we introduce the values of **Table 1**, in the geotherms (60) or (67), then in (57), we find that we are dealing with a bundle, and this for each site. The coefficients obtained from the geotherm of each, are different from another site in Kankule. We can then say that each site is a different bundle than that of a site from the same environment. Paragraph 2.1.4: The visualization of bundles by means of stereographic projection, allows us to say that two different bundles in circles, do not meet. Such a situation should be verified with the physical or chemical properties of the thermal waters of the sites. For that, we will have to check if at least one same source feeds two different sites. This could help us understand why each thermal bath in the world's largest power plant, The Geysers in the United States, exploits each source to generate electric current [25]. It is the same for the geothermal power station of Soultz for Alsace in France.

4.3. Comparison of Ion Density Values in Site Thermal Baths

Can we say that the same source of thermal water supplies two different sites? Here is the result which seems to appear from the study of **Table 3**. We have the same ions in all thermal waters: Cl^- (mg/L), SO_4^- (mg/L), HCO_3^- (mg/L), PO_4^- (µmol/L), NH_4^+ (µmole/L) and NO_3^- (µmol/L), which suggests that we have the same source everywhere. However, the analysis of the geological map of the DRC [30] or that of Kivu [31], what can we say? We are in the presence of the same recent basic lava. What our first impressions can only translate is that our Kankule thermal springs have only been in contact with the same source rock. To realize this, we divide the numerical data of the two parallel lines each time. If the results found give a value of 1 everywhere, then two different sites should be supplied by the same groundwater source. What we find as a result of the calculations, for example between Kankule I and II, are really different. We find that the ion concentrations or densities are very different between two different sites. We come to the conclusion that in depth, two different sources do not meet after being in contact with the heat coming from the magma chamber (or hot rock). In other words, deep heat islands of the same basalt, but differently heated at two different points, are sources of energy observable in Kankule through the thermal waters. This corroborates the idea of bundles discussed in the previous paragraph. In fibration language, what are we going to call the thermal water sites and the magma chambers that supply them? The visualization of fibration by stereographic projection, from paragraph 2.4.3., allows us to say that the deep magma chamber is the point above which the bundle is made. This hot rock is a source of heat, so we call it the heat core. The thermal water site, which is a bundle above the magma chamber, we call it bundle of heat.

Are there parallels between the heat bundles and the magnetic field lines?

The Hopf fibration of electromagnetic waves obtained by [27] and the one we obtained using relations (33), (36), (37) and (57), lead us to think that these two structures on S^3, have links. In an electromagnetic wave there is always an interaction between a magnetic field and an electric field. And this at all times. The results in **Table 3** help us to see that the heat from each Kankule site has contributed to the ionization of the thermal waters. There can then exist a certain bond between the geomagnetic field in a site with the field created by heat, represented by the temperature of the ground of the site of thermal baths. This observation leads us to discuss the results of **Table 2**. Is there a linear regression of the geomagnetic field B in temperature of the soil of the corresponding site? We are tempted to answer with yes when the null hypothesis Ho is accepted, and with no when this null hypothesis is rejected. In all cases, we arrive at a non-zero correlation between the temperature and the Earth's magnetic field of the corresponding site. We have found by way of illustration for Kankule I, using the R software, and exploiting the statistics, the following results:

```
>summary (dt1)
Call:
lm (formula = zmatrix.temp.champ1[, 1] ~ zmatrix.temp.champ1[, 2])
Residuals:
Min 1Q Median 3Q Max
−1.9712 −0.6506 0.0449 0.5635 3.7750
Coefficients:
Estimate Std. Error t value Pr (>|t|)
(Intercept) 4.964e−15 1.399e−01 0.000 1.000
zmatrix.temp.champ1[, 2] 5.196e−02 1.412e−01 0.368 0.714
Residual standard error: 1.009 on 50 degrees of freedom
Multiple R-squared: 0.0027, Adjusted R-squared: −0.01725
F-statistic: 0.1354 on 1 and 50 DF, p-value: 0.7145
```

Result that we can write

$$B = 5.196\text{th}-02T - 4.964\text{th}-15;\ 5\%. \tag{69}$$

In other words, the linear dependency hypothesis between B and T is accepted up to the 5% threshold. The B magnetic field is expressed in micron-Tesla and the temperature T in degrees Celsius. Matching the site's magnetic field with soil temperature *in situ* helps us understand how the geomagnetic field can model heat fiber. In this passage we bypassed the topological approach. Introducing (69) in (49), we find:

$$\frac{\partial^2 B}{\partial z^2} - \frac{1}{\alpha}\frac{\partial B}{\partial t} = 0 \tag{70}$$

This equation is that of Fourier, applied to the terrestrial geomagnetic field. She explains that the Earth's magnetic field is increasing from the surface of the ground to the center of the Earth, fact which is justified by the nonzero thermal gradient, or then the nonzero geomagnetic gradient, phenomenon that allows

various applications of geothermal energy [16]. From Maxwell's equations of the classical electromagnetic field, Faraday-Henry's law gives us:

$$\text{rot } E = -\frac{\partial B}{\partial t} \tag{71}$$

Equation expresses that the variation of the magnetic field in time generates the electric field. The integral solution of (70), being of type (50) or (57), then the earth's magnetic field is really a bundle. It is a Hopf fibration generated by Charge movements, according to Maxwell's equations. Our approach allows us to validate the Hopf fibration model that we carried out in paragraphs 2.1.3 and 2.1.4. Thus the electromagnetic waves are then modeled as a Hopf Fibration. This is also the result of the work of William T.M. and Dirk Bouwmeester [27]. And reciprocally, the linear links between B and T, allows us to corroborate the notion of fibration of the field T, for the site of Kankule I.

For the other Kankule sites, we had obtained similar results. Even if the null hypothesis is rejected, as in Kankule IV. There is always a certain linearity, as weak as it is, between the magnetic field of the site and the geomagnetic field. This implies that there is an interaction between the magnetic field of the site and the soil of the corresponding site, however small. Indeed, the ionization of thermal waters observed with the results of **Table 3**, allows the creation of the electromagnetic field in place [16]. And this field in thermal waters interacts with the geomagnetic field of the place. In view of the above, we can say that the geomagnetic field allows us to detect the state of electrification at any Kankule geothermal site. There is therefore parallelism, in terms of interaction, between the B and T fields of a given Kankule site.

4.4. Which Geothermy Could Be Exploited in Kankule?

The average Kankule thermal gradient of 0.117˚C/m differs from the global average thermal gradient of 0.033˚C/m. This Kankule gradient is 3.5 times greater than the global average thermal gradient. With this average Kankule thermal gradient, we should be able to exploit different types of geothermal energy as indicated [24]. The different types of geothermal energy that can be used in Kankule are:

- <30˚C and <500 m: surface geothermal energy. This takes up the very low temperatures (enthalpy). Because at 257 m deep, we will have temperatures of at most 30˚C.
- between 25˚C - 30˚C and 150˚C and >500 m: deep geothermal energy. Because at a depth of 500 m, we will already have a temperature of 58.5˚C. In order to generate electricity, it would have to be over 100˚C. By digging up to 1500 m, or 1.5 km, deep, we will have temperatures reaching 175.5˚C. Going up to 2000 m deep, we will have a temperature of 234˚C. The production of electricity is then possible from 50˚C as already pointed out [23].
- For Kankule IV, with a gradient of 125, 471, 195˚C/km. You can reach desired temperatures by drawing water more than 2 km deep, reaching temper-

atures of 234˚C. A good result when we already compare them to that of Soultz in France [25] [26].

5. Conclusions

In the present work, we have found that:

- Each thermal water site is represented by the temperatures of the soil or of its waters;
- Each site is a heat beam taken as a fibrous equivalent to a line of the magnetic field of the place;
- There is interaction between the bundle of the site's geomagnetic field and the bundle of heat.

Conflicts of Interest

The authors declare no conflicts of interest regarding the publication of this paper.

References

[1] Lyons, D.W. (2006) An Elementary Introduction to the Hopf Fibration. Lebannonn Valley College, Annville, 1-16.

[2] Kalongama, J.M. (2009-2010) Méthodes de Géométrie différentielle appliquées en Sciences Physique. Séminaire de DEA animé à l'UPN/ISP en RDC; Inédit.

[3] Lafuente-Gavy, L., *et al.* (2009) La fibration de Hopf. Université Libre de Bruxelles, Bruxelles, 26-36.

[4] Kalongama, J.M. (2007-2008) Sur la généralisation isotopique de la théorie quantique du moment angulaire. Thèse de doctorat défendue à l'UNIKIN.

[5] Faraut, J. (2006) Analyse sur les groupes de Lie. Calrenge &Mounet, Paris.

[6] Hladik, J., *et al.* (2009) Mécanique Quantique. Atomes et Noyaux: Applications. Dunod, Paris.

[7] Jean-François Arbour, UQAM (2012) S3 et la fibration de Hopf.

[8] https://fr.wikipedia.org/wiki/Projection_stérréographique

[9] Messiah, A. (1960) Mécanique Quantique, Tome 2. Dunod, Paris.

[10] Tannoudji, C.C., *et al.* (1977) Mécanique Quantique, Tome 2. Herman, Paris.

[11] Tannoudji, C.C., *et al.* (2007) Mécanique Quantique, Tome 2. Herman, Paris.

[12] http://www.dimensions-math.org/Dim_CH7.html

[13] Navez, J. (2009-2010) Théorie des groupes. Séminaire de DEA animé à l'UPN/ISP en RDC, Inédit.

[14] Mulenda, A. (2013) Modélisation du transfert des températures sol-air-eau thermale de Kankule dans Katana au Sud-Kivu. Mémoire de D.E.A présenté à l'Université Pédagogique Nationale de Kinshasa (UPN /Kin), Faculté des Sciences, Département de Physique.

[15] Finn, A., *et al.* (1986) Physique générale 1, Mécanique et thermodynamique. Inter Editions, Paris.

[16] Finn, A., *et al.* (1977) Physique générale 2, Champs et Ondes. Inter Editions, Paris.

[17] Reif, F. (1989) Physique statistique, Berkeley: Cours de Physique, Volume 5.

Armand Colin, Paris.

[18] Lavrentiev, M., *et al*. (1972) Méthodes de la théorie des fonctions d'une variable complexe. Mir, Moscou.

[19] Piskounov, N. (1972) Calcul différentiel et intégral, Tome 2. Mir, Moscou.

[20] Nofzinger, D.I., *et al*. (2003) Soil Temperature Change with Time and Depth: Theory.

[21] Chatterji, S.D. (1998) Cours d'Analyse. 3 Equations différentielles ordinaires et aux dérivées partielles. Presses Polytechnique et Universitaires romandes, Bienne.

[22] Koudriatsev, V., *et al*. (1986) Cours élémentaire de mathématiques supérieures. Mir, Moscou.

[23] Géosciences (2013) La revue du BRGM pour une Terre durable, No. 16.

[24] Ecorem, S.A. (2011) Etude des obstacles à la géothermie profonde (basse et haute énergie). Rapport final, Département de l'énergie, Wallonie.

[25] https://fr.wikipedia.org/wiki/Géothermie

[26] Boden, J.-P., *et al*. (1988) Biologie et Géologie, Première S. Bordas, Paris.

[27] Irvine, W.T.M. and Bouwmeester, D. (2008) Linked and Knotted Beams of Light. *Nature Physics*, **4**, 716-721. https://doi.org/10.1038/nphys1056

[28] http://www.geologie.ens.fr

[29] http://www.arl.noaa.gov/ready.geomagn

[30] Musée Royal de l'Afrique Central (2005) Carte géologique de la République Démocratique du Congo, Tervuren.

[31] De la carte géologique du Sud-Kivu, 1939.

Symbols Used

q: quaternion

(a, b, c, d): unit quaternion

S^n: sphere unit of dimension n

$\psi_{N'}$: stereographic projection in R^2 from the North Pole N'

φ_N: stereographic projection in R^3 from North Pole N

i: imaginary unit

T: temperature

$\overline{T_0}$: average annual soil temperature

$\overline{A_0}$: the annual average thermal amplitude

d: damping depth

α: thermal diffusivity coefficient

z: depth in the ground

ω: annual pulse of thermal waves

B: module of the Earth's geomagnetic field

t: time

σ: temperature variance